polymers

MDPI

Article

New Type of Free Radical Photopolymerization Photoinitiator Based on Bisacylphenylphosphine Oxide

Yinping Wu [1,2,*], Zhiqiang Zhou [1], Aihuan Gao [1], Shuyi Zhang [1], Yanjuan Li [1], Bo Zhang [1,*] and Xiang Li [1,*]

[1] School of Environmental and Chemical Engineering, Zhaoqing University, Zhaoqing 526061, China; 18666237344@163.com (Z.Z.); gaoaihuan@zqu.edu.cn (A.G.); 15992264226@163.com (S.Z.); 14754681402@163.com (Y.L.)
[2] New Energy and New Materials Research Center, Zhaoqing University, Zhaoqing 526061, China
* Correspondence: wuyinping@zqu.edu.cn (Y.W.); zhangbo2018@zqu.edu.cn (B.Z.); lix@zqu.edu.cn (X.L.)

Abstract

This paper designed and synthesized four types of I-type free radical photoinitiators (BTBOL-1 to BTBOL-4) containing two acylphosphine oxide structures, which were used for UV-LED photopolymerization reactions. Four different chain-length ethylene glycol substituents were introduced into the molecular structure to form a series of bisacylphosphine oxide photoinitiators. The chain-length dependence of the ethylene glycol substituent on photoinitiator performance was investigated in terms of UV–vis absorption, steady-state photolysis, photopolymerization behavior, monomer solubility, and mobility. The four new types of photoinitiators BTBOL-1/BTBOL-2/BTBOL-3/BTBOL-4 not only have good solubility in acrylic monomers, but also exhibit excellent photopolymerization performance. Moreover, through extraction method and ultraviolet-visible spectroscopy technology, it was detected that their migration rate in the cured film is lower than the detection limit. Compared with the conventional commercial photoinitiator TPO-L (migration ratio: 0.98%), the high-molecular-weight diacylphosphine oxide exhibited superior migration stability. These findings indicate that BTBOL-1–BTBOL-4 hold considerable promise as type I radical photoinitiators for low-migration UV-LED photopolymerization systems.

Keywords: biacylphosphine oxide; low migration; type I photoinitiator; good solubility

1. Introduction

Photopolymerization is recognized as a green, highly efficient, and readily controllable polymerization process [1], and it has drawn substantial attention in both industrial and scientific communities in recent years [2,3]. This technique harnesses light to achieve exact spatial and temporal control, and it is characterized by low energy requirements and the absence of any need for high-temperature operation. Currently, photopolymerization technology is broadly employed in ink coatings [4–6], photoresists [7,8], 3D printing [9], biomaterials [10], dental materials [11], and optoelectronic devices [12], and it not only improved production efficiency [13] but also contributed positively to environmental sustainability [14–16]. The photoinitiator dictates the wavelength range absorbed, the efficiency of the photopolymerization reaction, and the physical properties of the final coating; therefore, it plays a pivotal role in the formulation [17–20].

The photoinitiator is a crucial component in photopolymerization reactions. It can generate active substances upon light exposure, thereby inducing the polymerization reaction of monomers. Depending on the mode of radical formation, organic carbonyl photoinitiators are broadly categorized into two families, Type I (photo-induced α-elimination) and Type II

Check for updates

Academic Editor: Yung-Chung Chen

Received: 17 October 2026
Revised: 19 November 2026
Accepted: 26 November 2026
Published: 28 November 2026

Copyright: © 2026 by the authors. Licensee MDPI, Basel, Switzerland. This article is an open access article distributed under the terms and conditions of the Creative Commons Attribution (CC BY) license.

(photo-excitation hydrogen abstraction) [21]. Type I photoinitiators mainly include acetylbenzene derivatives, benzeneethers, amino ketones, and acylphosphine oxides [22,23]. The deeper penetration achieved by LEDs—a result of their longer wavelengths and lower photon energies relative to traditional UV sources is favourable for complete curing of thick composite materials. Meanwhile, LED sources inflict significantly less photodamage on human tissues and polymeric materials compared to mercury lamps [24,25]. TPO-L(Ethyl (2,4,6-trimethylbenzoyl) phenylphosphonic acid ester) is a commercially available acylphosphine oxide photoinitiator with excellent solubility, high photoinitiating efficiency, and applicability to UV-LED light sources. Although TPO-L exhibits the highest reactivity, TPO-L suffer from high migration issues [26]. Upon photoexcitation, the acyl phosphine oxide photoinitiator is promoted to an excited singlet state, which then converts to the triplet state through intersystem crossing (ISC). The C-P bond is cleaved, delivering two free radicals, namely an acyl radical and a phosphorus-centered radical. Both carbon-centered free radicals and phosphorus-centered free radicals can trigger polymerization reactions [27]. As typical Type I photoinitiators, acylphosphine oxides (APOs) exhibit intense absorption in the ultraviolet to near-ultraviolet range, excellent reactivity, and satisfactory photobleaching behavior [28–31]. APOs are regarded as the most attractive category of free radical Type I photoinitiators suitable for UV-LED light sources [32,33]. Nevertheless, acylphosphine oxides suffer from several limitations, including weak absorption in the visible region, susceptibility to oxygen inhibition, poor solubility in resin, and migration of the unreacted species [34,35].

The migration of photoinitiators that did not participate in the crosslinking reaction from the network structure of the cured coating remains a key challenge, as it often damages the surface smoothness of the coating and contaminates the substrate it comes into contact with. Therefore, in applications such as light-cured wood coatings, adhesives, and inks, light initiators with high migration rates encounter numerous application limitations [36–39]. Consequently, the design of acylphosphine oxide photoinitiators combining high initiation efficiency with low migration propensity has emerged as a key research priority, though substantial hurdles remain [40,41]. A reasonable molecular design must take into account the absorption wavelength, the light-initiation efficiency, and the solubility of the monomer. Moreover, ensuring the low mobility of the photoinitiator is another important issue that must be prioritized in future design work. This work is primarily directed toward lowering the migration propensity of the acylphosphine oxide photoinitiator.

Several studies have modified the benzoyl part of the acylphosphine structure to achieve specific improvements, such as reducing the mobility. Two strategies have been proposed to overcome the high mobility of photoinitiators. The first relies on increasing molecular weight, e.g., through the design of high-molecular-weight photoinitiators. Qu [40] modified the benzoyl group to a triphenylamine (NHPO) or pyrene group (BHPO), and the maximum absorption peak of the resulting acyl-oxygen phosphine photoinitiator shifted to 419 nm and its mobility was reduced to 0.23%. Qu [41] modified the benzoyl group to a thienazine group to prepare the acyl oxygen phosphine photoinitiator, which caused the maximum absorption peak to shift to 667 nm and the mobility to decrease to 0.22%.

Another strategy is to introduce polymerizable groups, an approach that has attracted considerable attention in recent studies. Our group has previously prepared three classes of acylphosphine oxide photoinitiators [29,42], (allyl)carbazolyl derivatives, etheroxybenzoyl phosphine oxides absorbing at 350–420 nm, and low-mobility Type I APOs. In addition, the acylphosphine oxide chromophore has been functionalized with amine [43] and vanillin [44]. Such strategies were developed to improve both the safety and the performance of photopolymerization across diverse applications.

Recently, several researchers have modified the phosphonyl group in the acylphosphine oxide structure to achieve high initiation efficiency. Knaack [45] synthesized a series

of acylphosphine oxides with different phosphonyl groups, which exhibited absorption maxima at 385 nm. Xiao [46] designed and synthesized an acylphosphine oxide structure, TDOPO, which exhibited superior biocompatibility and photoinitiation efficiency compared to TPO. Wang [47] prepared two acylphosphine oxide derivatives bearing methyl substituents on the phosphonyl moiety, which exhibited both high photoinitiation efficiency and reduced migration. Lalevée and colleagues [27] have demonstrated that DOPO-based acylphosphinate photoinitiators, featuring a phosphinyl structure, exhibit good photopolymerization efficiency and significantly lower cytotoxicity than commercial TPO, and their experimental results confirm the potential of the DOPO scaffold as a functional core for designing novel, efficient, and low-toxicity Type I acylphosphine oxide photoinitiators.

Research has shown that increasing the molecular weight of the photoinitiator can reduce its mobility. However, a problem arises when the molecular weight is too high. Under the same mass addition amount, the photoinitiation efficiency of the high-molecular-weight photoinitiator is considerably lower than that of its low-molecular-weight counterpart. The ethoxy linker plays an essential part in enhancing the solubility [29]. The flexible polar poly(ethylene glycol) segments enhance the overall polarity and flexibility of the molecules, making the photoinitiators(BTBOL-1/BTBOL-2/BTBOL-3/BTBOL-4) more compatible with hydrophobic acrylic monomers and systems with higher polarity. The objective of this experiment is to increase the number of initiating groups in the macromolecular photoinitiator, thereby reducing the mobility of the photoinitiator. In this study, four novel acylphosphine oxide photoinitiators (BTBOL-1/BTBOL-2/BTBOL-3/BTBOL-4) were designed and synthesized, as shown in Figures 1 and 2. The photophysical, photochemical and mobility properties of the BTBOL-1/BTBOL-2/BTBOL-3/BTBOL-4 and TPO-L were evaluated.

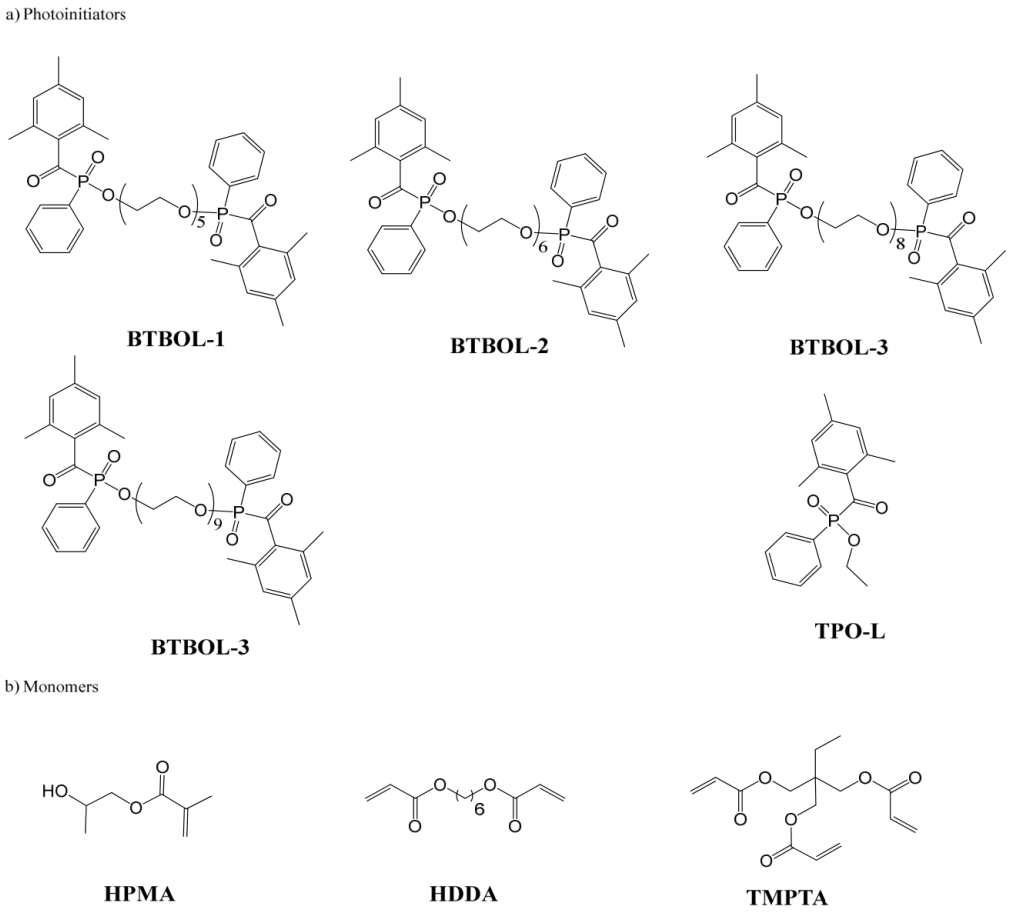
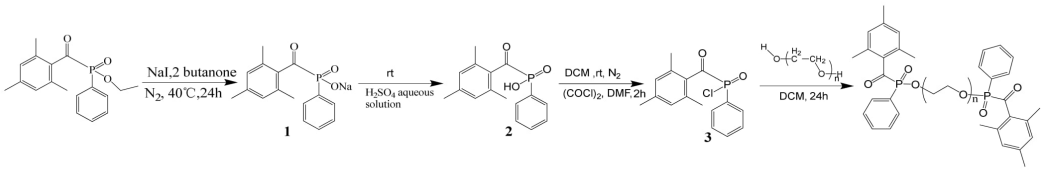


Figure 1. Molecular structures of photoinitiators and the monomers used in this study.



BTBOL-1: n = 5; BTBOL-2: n = 6; BTBOL-3: n = 8; BTBOL-4: n = 9;.

Figure 2. Synthetic route for the BTBOL1-4.

2. Results and Analysis

2.1. Optical Properties

The UV-Vis absorption characteristics of TPO-L and BTBOL-1/BTBOL-2/BTBOL-3/BTBOL-4 in CH_3CN are presented in Figure 3 and summarized in Table 1. Figure 3 presents the absorption features of BTBOLs over the 320–450 nm wavelength range. The maximum absorption peaks of BTBOL and TPO-L are both located at 370 nm. The molar absorptivity of BTBOL-1/BTBOL-2/BTBOL-3/BTBOL-4 are approximately or even twice that of TPO-L, indicating that as the ethoxy chain segments increase, the molar absorptivity of them gradually increases. The results demonstrate that BTBOL-1/BTBOL-2/BTBOL-3/BTBOL-4 possess great promise as photoinitiators compatible with near-UV LED irradiation.

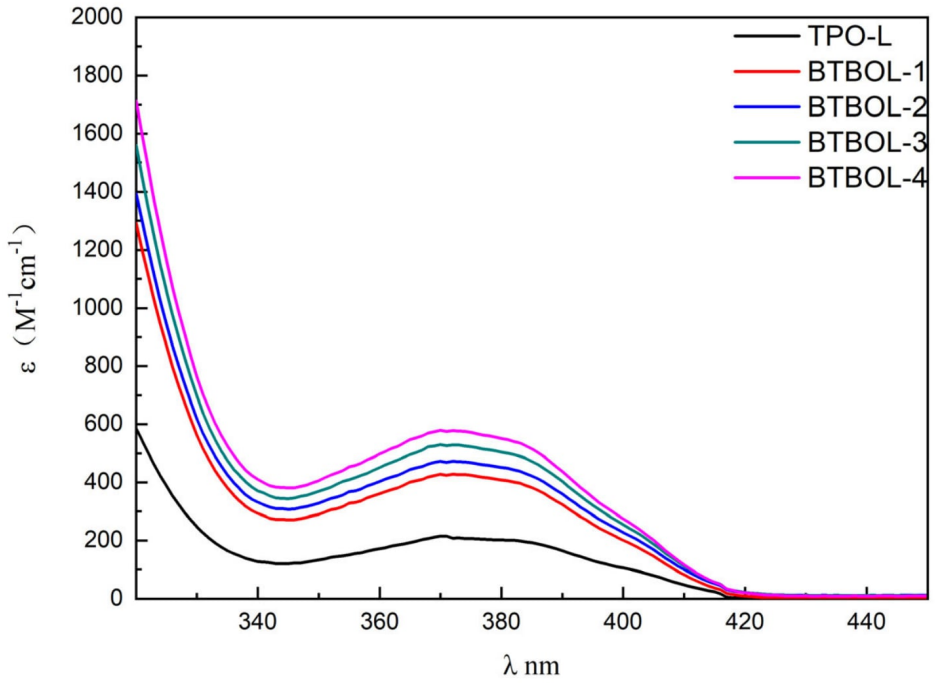


Figure 3. UV–vis absorption spectra of BTBOLs dissolved in CH_3CN.

Table 1. Photophysical data for BTBOLs.

PIs	λ_{max} (nm)	ε_{max} ($Lmol^{-1}cm^{-1}$)	ε_{365} ($Lmol^{-1}cm^{-1}$)	ε_{385} ($Lmol^{-1}cm^{-1}$)	ε_{405} ($Lmol^{-1}cm^{-1}$)	λ_{em} (nm)	Egap (eV)	Φ
TPO-L	370	215	193	193	80	448	4.73	0.12
BTBOL-1	370	428	404	382	146	427	4.23	0.13
BTBOL-2	370	473	445	423	169	426	4.14	0.15
BTBOL-3	370	530	496	473	187	428	4.22	0.12
BTBOL-4	370	579	547	516	201	425	4.57	0.12

Where ε is the molar extinction coefficient, λ_{em} is the fluorescence emission maximum of the photoinitiators, and E_{gap} refers to the HOMO–LUMO energy gap.

Fluorescence spectroscopic measurements (Figure 4, Table 1) were carried out to explore the excited-state characteristics of BTBOLs. The lower fluorescence intensity indicates that the main pathway for the deactivation of the excited states of BTBOLs and TPO-L is non-radiative transition [48].

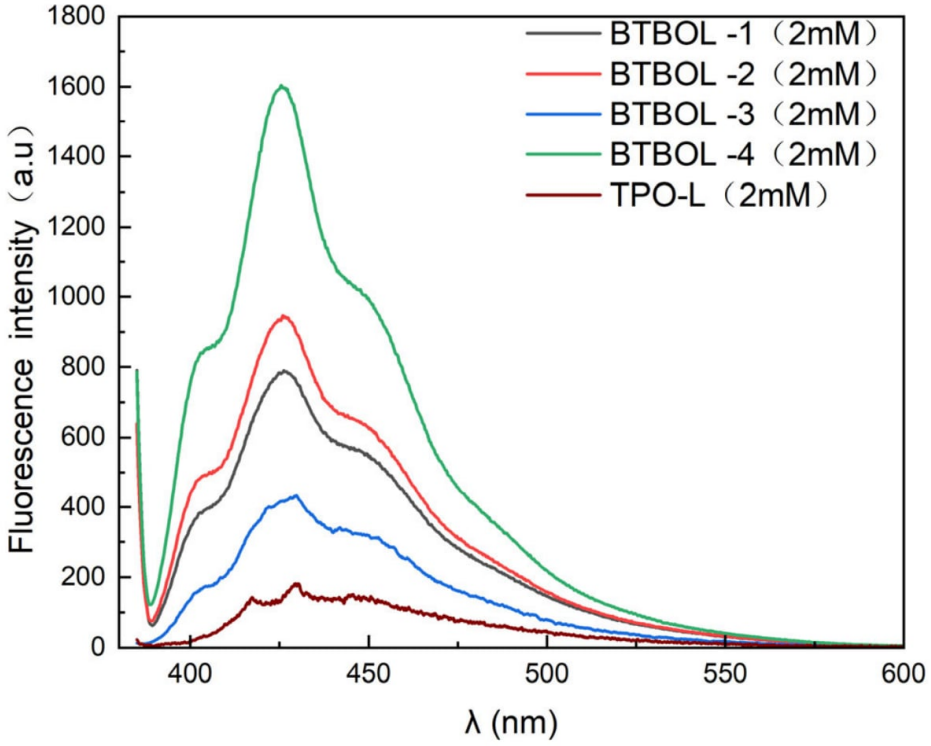
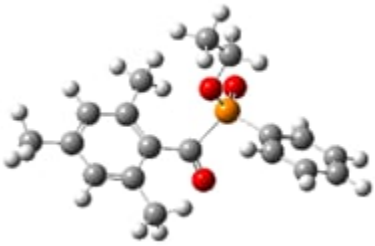
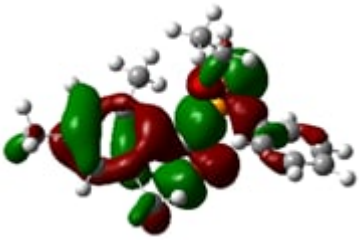
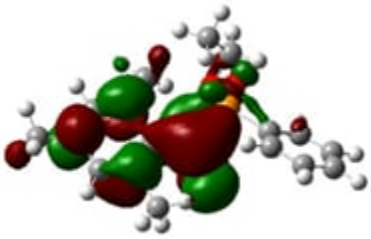
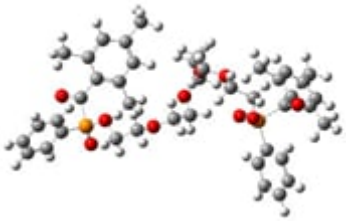
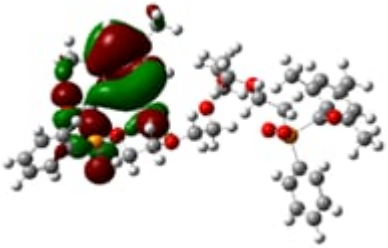
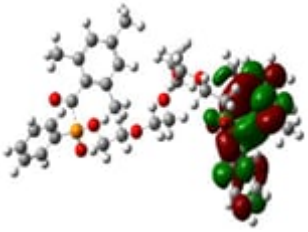
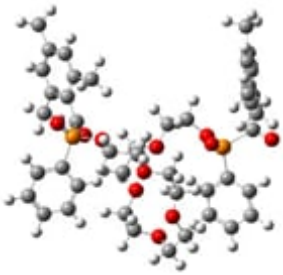
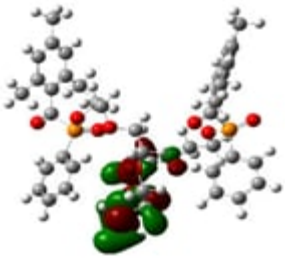
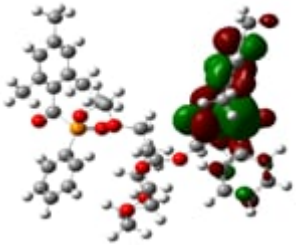
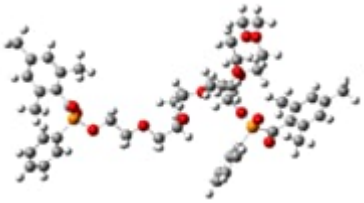
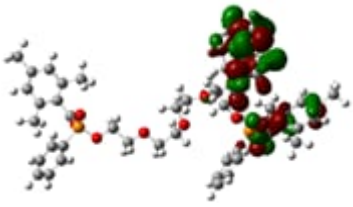
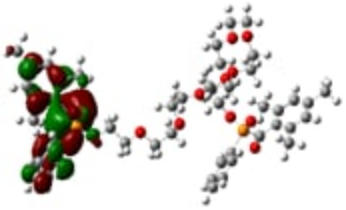
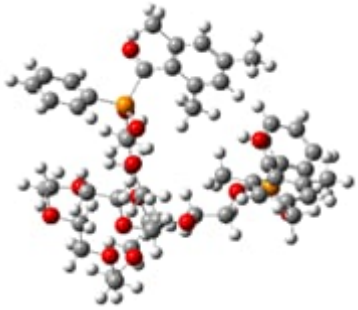
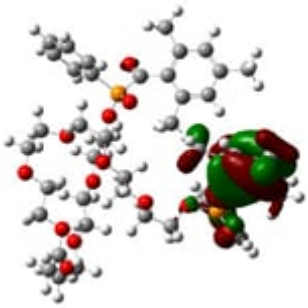
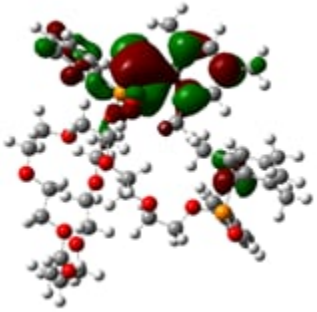


Figure 4. Fluorescence emission spectrum of BTBOLs and TPO-L in CH_3CN.

The molecular geometries of BTBOLs were optimized at the theoretical level using Gaussian, with the aim of elucidating their intramolecular charge transfer and electronic transition behavior. The frontier molecular orbital (FMO) energy levels were calculated via Gaussian package. Table 2 summarizes the calculation of the HOMO/LUMO energy levels of BTBOLs. According to Table 2, the HOMO electron densities of BTBOL-1, BTBOL-3, and BTBOL-4 are primarily situated on the oxygen atoms of the P=O and C=O groups. The LUMO energy level diagrams of BTBOLs have electron clouds mainly distributed on the C=O of the terminal trimethylbenzoyl group and the π framework of the benzene ring. For BTBOL-2, the HOMO electron density resides on the O atoms of the ethoxy linker, whereas the LUMO is mainly situated on the benzoyl benzene ring and its C=O moiety. The energy level orbital separation of BTBOL-2 implies that the lowest energy level transition exhibits significant intramolecular charge transfer characteristics. During excitation, the electron distribution shifts from the connecting part to the benzoyl part. Nevertheless, this transition can still be classified as n→ π*, where the ethoxy oxygen atom acts as the electron donor (n-type orbital), and the benzoyl fragment acts as the acceptor (π* type orbital). This electronic property is expected to facilitate efficient Norris I-type cleavage, as the excitation is concentrated on the benzoyl phosphoranyl conjugated system. DFT calculations reveal that the lowest-energy electronic transition of BTBOLs is predominantly n→π* in character. The electron cloud of the LUMO level is mainly concentrated on the benzoyl group, confirming that this group undergoes a Norris I-type photolysis reaction. The ethoxy spacer chain lengths of BTBOLs are different, but their n→π* transition energy gaps are 4.23, 4.14, 4.22, and 4.57 eV respectively, remaining basically unchanged (Table 1). Except for BTBOL-4, whose energy gap is larger and close to 4.74 eV of TPO-L, the other results indicate that the influence of the ethoxy chain length on the n→π* transition is relatively small.

Table 2. HOMO-LUMO spatial localization and band-gap comparison between BTBOLs and TPO-L.

PIs	Optimized Structures	HOMO	LUMO
TPO-L		 E = −6.43 eV	 E = −1.69 eV
BTBOL-1		 E = −6.18 eV	 E = −1.95 eV
BTBOL-2		 E = −6.03 eV	 E = −1.88 eV
BTBOL-3		 E = −6.17 eV	 E = −1.95 eV
BTBOL-4		 E = −6.17 eV	 E = −1.60 eV

2.2. Photochemical and ESR-ST

Steady-state photolysis experiments were carried out to probe the photochemical behavior of the PIs. The corresponding absorption spectral changes in the photoinitiator in acetonitrile under 365 nm LED irradiation are presented in Figure 5. The four BTBOLs (BTBOL-1 to BTBOL-4) exhibit rapid photodegradation under the 365 nm LED irradiation light source, and their absorbance in the 360–410 nm wavelength range gradually decreases. The absorbance

at the absorption maximum (370 nm) of BTBOLs dropped to half of its initial value within 30 s of irradiation, and similar decreases were observed for all derivatives, confirming their rapid photodegradation. The spectral attenuation results collectively indicate that during the LED illumination process, due to the decomposition reaction of BTBOLs, the newly generated substances do not have absorption peaks within the 360–410 nm wavelength range, indicating that all BTBOLs have undergone irreversible degradation reactions.

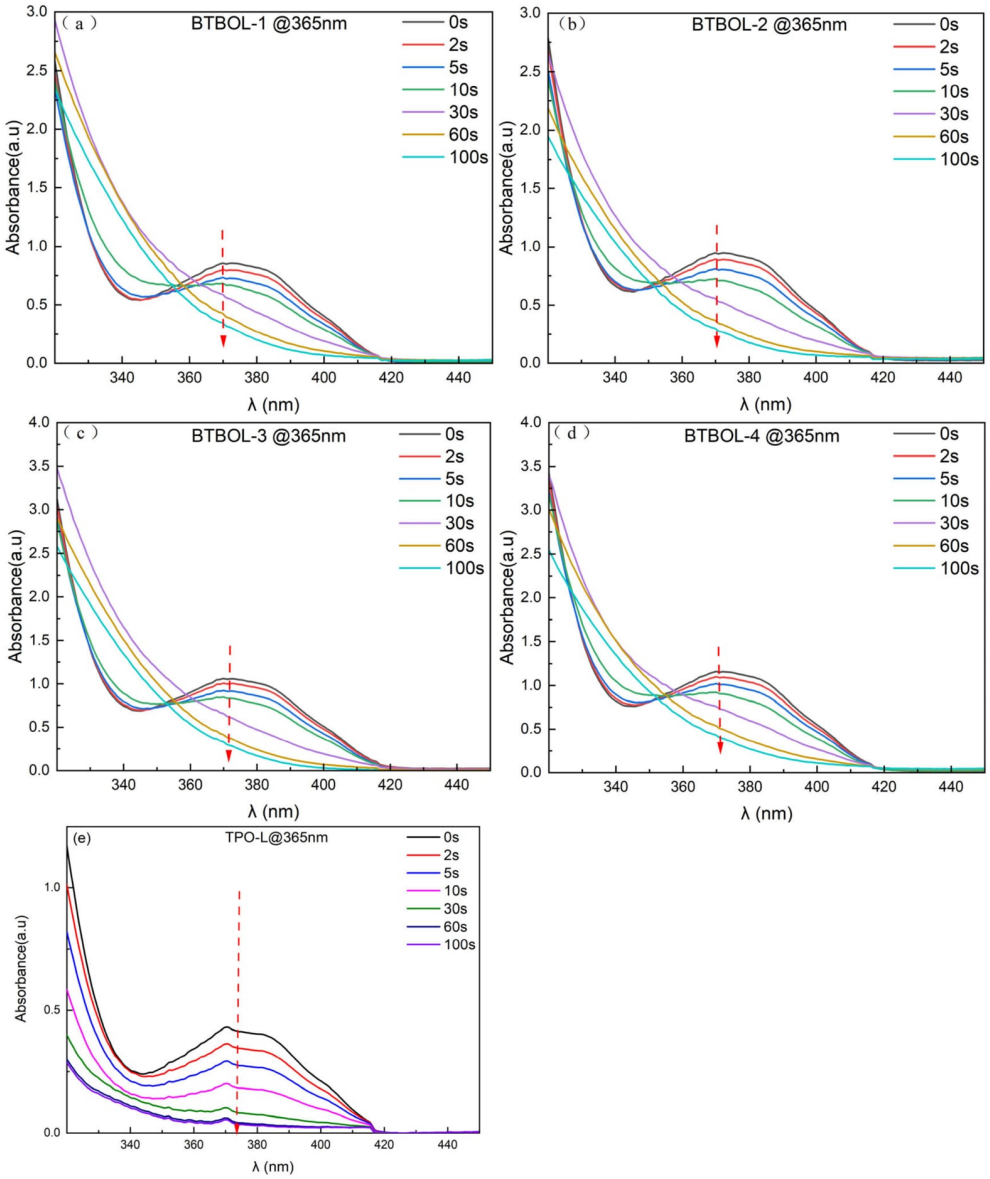


Figure 5. The steady-state photolysis reaction were recorded under LED@365 nm with a photoinitiator concentration of 2 mM in acetonitrile, (**a**) BTBOL-1, (**b**) BTBOL-2, (**c**) BTBOL-3, (**d**) BTBOL-4, (**e**) TPO-L.

The efficiency of α-cleavage was assessed via the quantum yield (ϕ), expressed as the number of molecules cleaved per photon absorbed, under photolysis conditions in acetonitrile (Table 1, Figure 6). As shown in Figure 6 and Table 1, BTBOL-2 exhibited the highest quantum yield ($\phi = 0.15$), indicating the most efficient generation of radicals per absorbed photon among the series. The remaining derivatives BTBOL-1 ($\phi = 0.13$), BTBOL-3 ($\phi = 0.12$), and BTBOL-4 ($\phi = 0.12$)—displayed quantum yields comparable to that of the reference photoinitiator TPO-L ($\phi = 0.12$), suggesting similar efficiencies in radical production upon

light absorption. Ultimately, only polymerization experiments can reveal the actual efficiency of these acylphosphine oxides and distinguish their photoinitiation behavior.

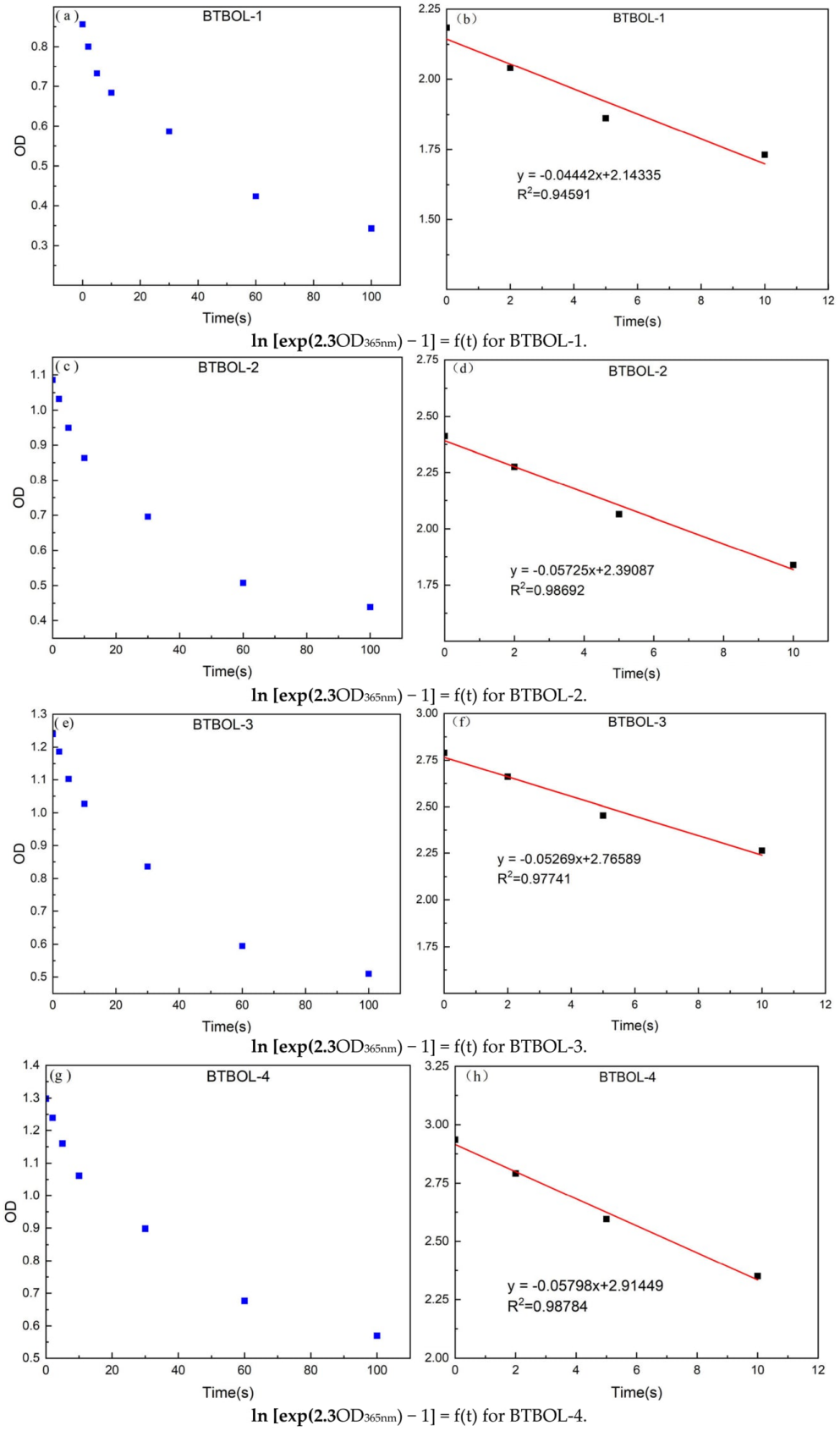


Figure 6. *Cont.*

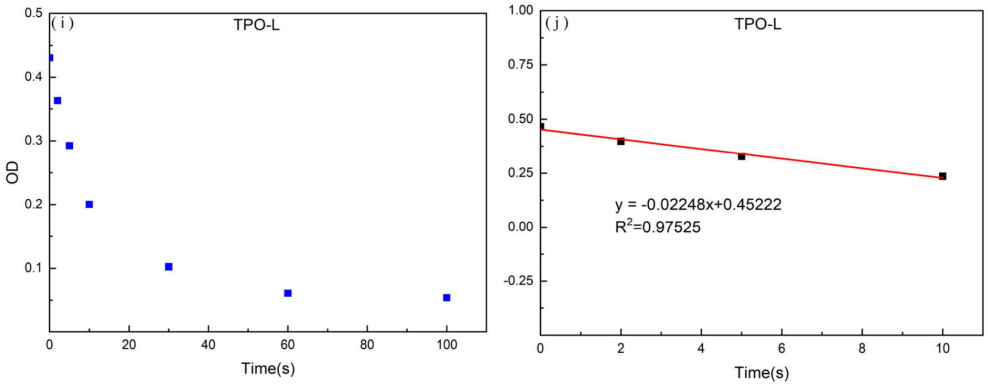


Figure 6. (**a**,**c**,**e**,**g**,**i**): evolution of the optical density (OD) at 370 nm of BTBOL-1, BTBOL-2, BTBOL-3, BTBOL-4 and TPO-L solution in acetonitrile upon exposure to a LED at 365 nm; (**b**,**d**,**f**,**h**,**j**) slope of the function ln[exp(2.3OD365 nm) − 1] = f(t) at the beginning of the reaction (slope of −0.04442 for BTBOL-1, −0.05725 for BTBOL-2, −0.05269 for BTBOL-4, −0.02248 for TPO-L).

To gain further insight into the photolysis of BTBOLs, ESR spin-trapping experiments were carried out to identify the radical species formed upon α-cleavage of the photoinitiators under 365 nm LED irradiation (Figures 7 and 8). The results showed that PBN could trap the phosphono● radicals formed after cleavage of the C-P bond, confirming that the photolysis process illustrated in Figure 8 does produce free radicals. The hyperfine splitting constants (hfsc) of the phosphinoyl radicals arising from α-cleavage of the five photoinitiators (TPO-L, BTBOL-1/BTBOL-2/BTBOL-3/BTBOL-4) were comparable. Representative parameters are listed for TPO-L (α_P = 2.15 MT, α_H = 0.26 MT, α_N = 1.41 MT), BTBOL-1 (α_P = 2.09 MT, α_H = 0.29 MT, α_N = 1.43 MT) BTBOL-2 (α_P = 2.10 MT, α_H = 0.29 MT, α_N = 1.43 MT), BTBOL-3 (α_P = 2.13 MT, α_H = 0.27 MT, α_N = 1.42 MT), BTBOL-4 (α_P = 2.12 MT, α_H = 0.29 MT, α_N = 1.42 MT).

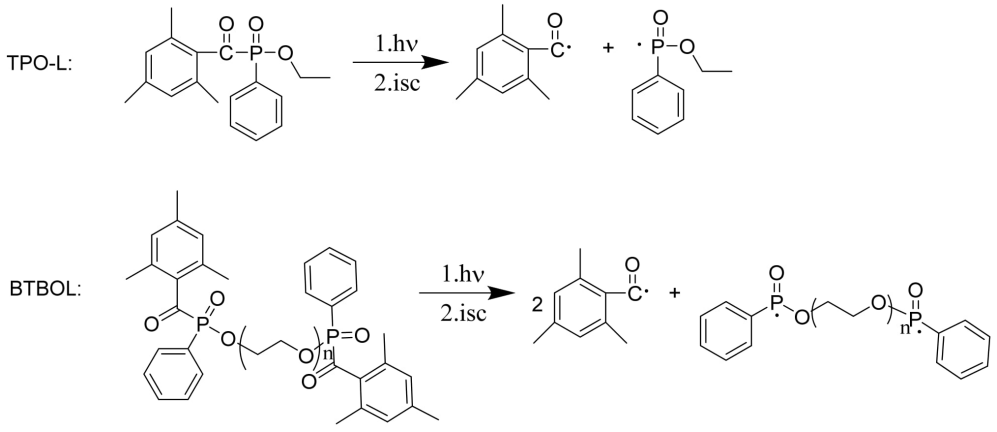


Figure 7. Proposed cleavage mechanism for BTBOLs.

2.3. Photopolymerizations

Through photopolymerization experiments (Figures 9 and 10 and Table 3), the photopolymerization efficiency of the monomer (TMPTA) system with 1 wt% photoinitiator BTBOLs under different light sources (365 nm and 405 nm LED irradiation) was investigated. Under the condition of LED@365 nm (100 mW/cm^2), in the TMPTA system, BTBOLs outperformed TPO-L in terms of double bond conversion (DC_{120}), except for BTBOL-2 (68.83%), where BTBOL-1 reached 73.84%, higher than the 70.35% of TPO-L. The DC of BTBOL-3 and BTBOL-4 were 77.3% and 76.63% respectively, and their photoinitiation efficiencies DC

all exceeded 70%. At 405 nm (50 mW/cm^2) in TMPTA, BTBOLs exhibited higher DC than TPO-L, except for BTBOL-2, where BTBOL-1 reached 70.48%, higher than the 70.35% of TPO-L; the DC of BTBOL-3 and BTBOL-4 were 73.85% and 76.88% respectively, and their photoinitiation efficiencies all exceeded 70%. The polymerization rate is shown in Figure 10. Under the LED@365 nm illumination, the order of the polymerization rates of BTBOLs is BTBOL-4 ≈ BTBOL-3 > BTBOL-1 > TPO-L ≈ BTBOL-2. Additionally, under the LED@405 nm illumination, the order of the polymerization rates of BTBOLs is BTBOL-4 > BTBOL-3 ≈ BTBOL-1 ≈ TPO-L > BTBOL-2. Under the irradiation of LED@365nm and LED@405nm, BTBOL-1, BTBOL-3 and BTBOL-4 may potentially serve as substitutes for TPO-L.

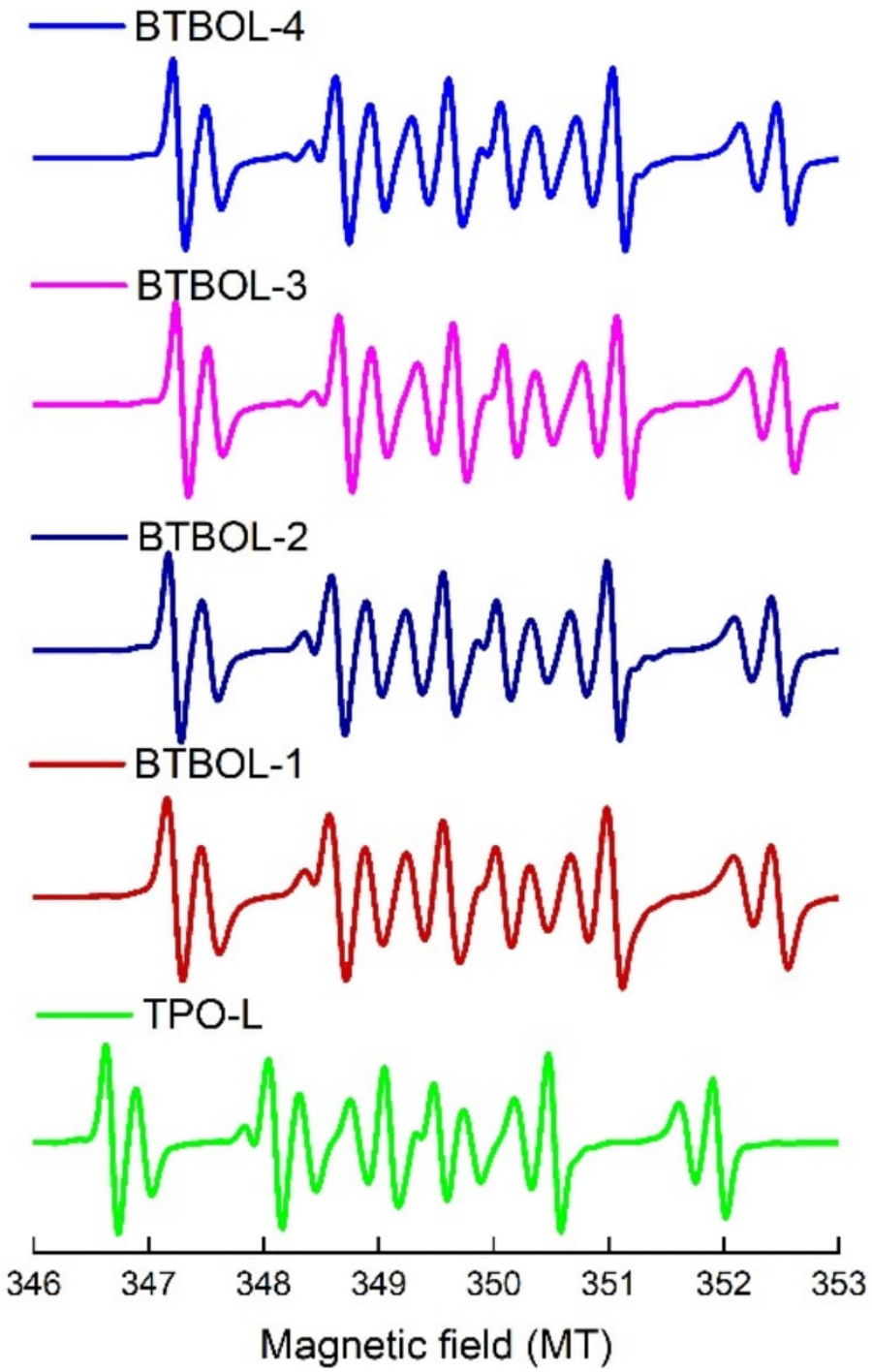


Figure 8. ESR-ST of BTBOLs and TPO-L.

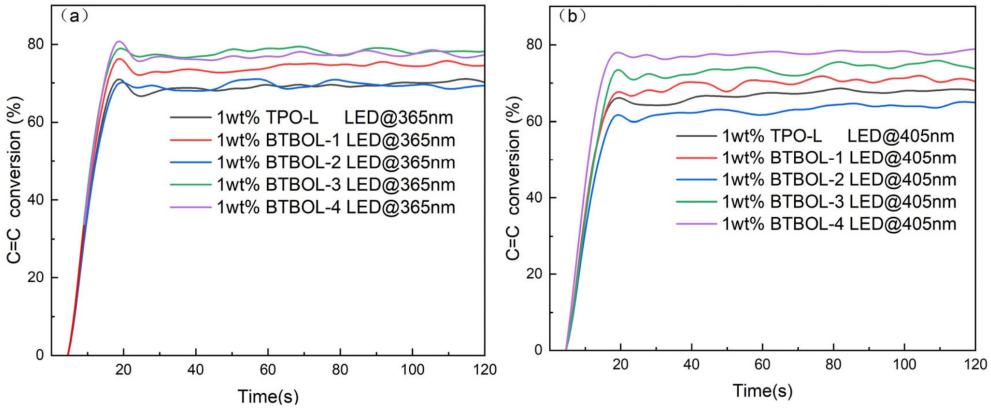


Figure 9. Conversion profiles of PIs in TMPTA (1 g PI/100 g TMPTA): (**a**) TMPTA under LED@365 nm; (**b**) TMPTA under LED@405 nm.

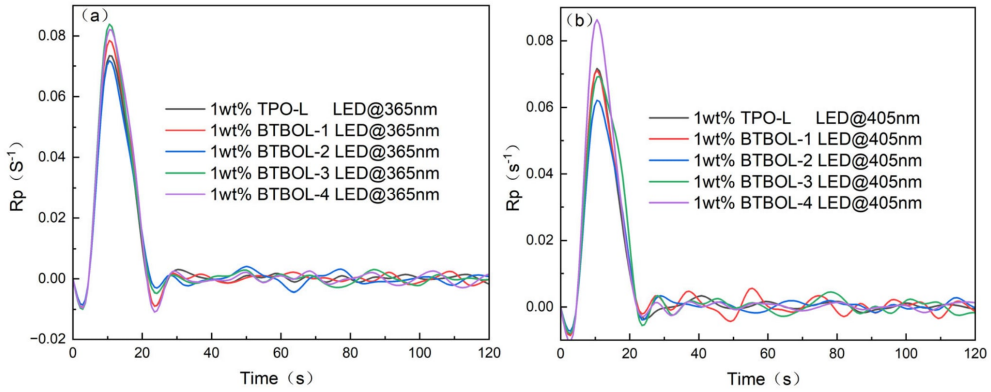


Figure 10. The photopolymerization rate of BTBOLs systems (**a**) TMPTA under 365 nm LED irradiation; (**b**) TMPTA under 405 nm LED irradiation.

Table 3. The degree of C=C conversion (DC_{120}) during photopolymerization.

PIs	DC_{120} (365 nm)	DC_{120} (405 nm)
1 wt% TPO-L	70.35%	68.41%
1 wt% BTBOL-1	73.84%	70.48%
1 wt% BTBOL-2	68.83%	63.93%
1 wt% BTBOL-3	77.30%	73.85%
1 wt% BTBOL-4	76.63%	76.88%

2.4. Solubility

Good miscibility of photoinitiators with photopolymerizable acrylate monomers and oligomers is essential for their practical application. Unfortunately, the low solubility of many newly developed high-performance photoinitiators remains a major obstacle to their industrial translation. To assess their processability, the solubility of BTBOLs and commercial TPO-L was tested in representative monomers (HPMA, HDDA, and TMPTA), and the comparative data are given in Table S1. The solubility of BTBOLs in the three monomers were comparable to that of commercial TPO-L. Owing to their liquid nature at ambient temperature, BTBOLs are highly miscible with all three liquid monomers. TPO-L has been widely used because its liquid state eliminates the need for pre-heating or the addition of diluents prior to industrial application, thereby reducing the cost of photocurable formulations. Moreover, the coatings cured with TPO-L exhibit excellent properties such as high hardness, further contributing to its widespread adoption. The BTBOLs synthesized in this experiment contain a diacylphosphine oxide structure and have an ethoxy-long-chain

introduced. The ethoxy linker contributes significantly to the enhanced solubility. The flexible polar poly(ethylene glycol) segments enhance the overall polarity and flexibility of the molecules, making the photoinitiator BTBOLs more compatible with hydrophobic acrylic monomers and systems with higher polarity [29]. The liquid nature of BTBOL-1, BTBOL-2, BTBOL-3 and BTBOL-4, together with their excellent solubility in photocurable monomers, renders them advantageous for industrial use. From the perspective of solubility, all BTBOLs are promising candidate materials for replacing TPO-L.

2.5. Migration of BTBOLs

The significant migration of photoinitiators poses a major obstacle to their application in the fields of coatings, inks, and adhesives in the photopolymerization industry. The migration rate test results of BTBOLs are shown in Figure 11 and Table 4. According to Table 4, the migration rates of BTBOL-1, BTBOL-2, BTBOL-3 and BTBOL-4 are all 0.00%, which are below the detection limit and much lower than that of TPO-L (0.98%). The migration stability of photoinitiators can be improved by increasing their molecular weight. Accordingly, the BTBOLs, with molecular weights ranging from 777.31 to 953.41 g/mol (versus 316.34 g/mol for TPO-L), exhibit significantly suppressed migration. These results suggest that BTBOLs hold great potential for applications in coatings, inks and adhesives, where low migration is essential.

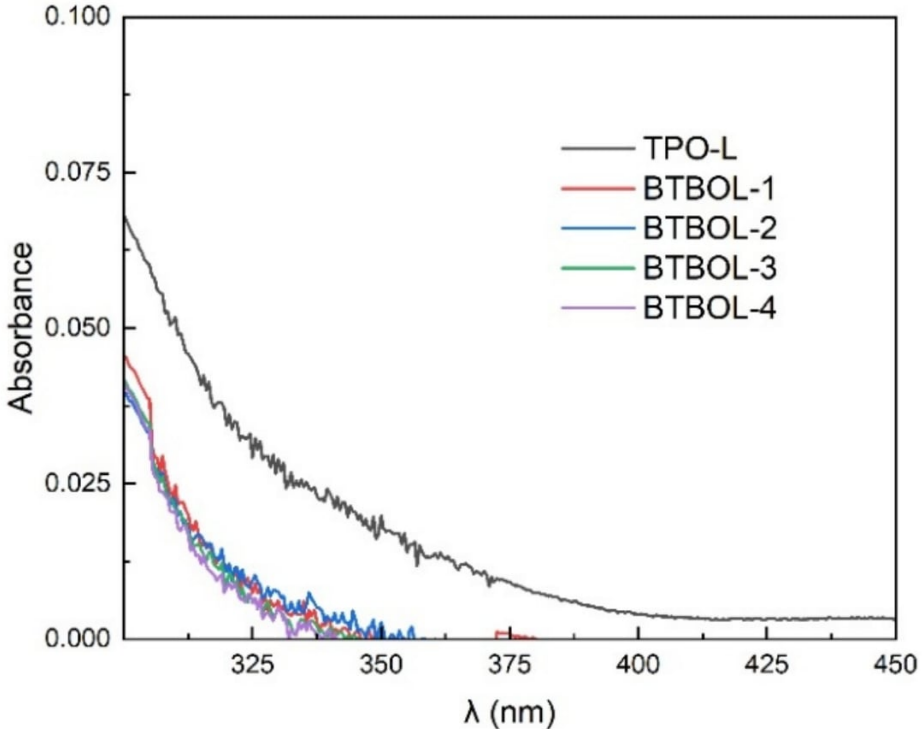


Figure 11. Absorbance of PIs extracted from cured films in acetonitrile.

Table 4. Migration behavior of BTBOLs.

PIs	A (a.u)	m (mg)	λ_{max} (nm)	M_r (g/mol)	ε_{max} ($Lmol^{-1}cm^{-1}$)	Migration Ratio
BTBOL-1	0.0000	887.2	370	777.31	428	0.00%
BTBOL-2	0.0000	708.7	370	821.33	473	0.00%
BTBOL-3	0.0000	713.7	370	910.97	530	0.00%
BTBOL-4	0.0000	752.8	370	953.41	579	0.00%
TPO-L	0.0085	637.2	370	316.34	215	0.98%

2.6. Comparison with Previously Reported Glycol-Linked Bis(acylphosphine oxide) Photoinitiators

The present photoinitiators are structurally related to the BTPO1–3 series reported in Reference [29], in which three bis(acylphosphine oxide) photoinitiators are linked by glycol chains with 3, 4, and 7 ethylene glycol units. The present work extends this series to chain lengths of 5, 6, 8, and 9 ethylene glycol units, enabling a direct comparison of structure–property relationships across a broader chain-length range. Several trends emerge from this comparison. First, in terms of synthetic accessibility, the yield decreases progressively with increasing glycol chain length in both series, and chains longer than 10 ethylene glycol units become extremely difficult to synthesize. The present chain lengths (5–9 units) therefore lie in a practically accessible window that balances synthetic feasibility against the property benefits of longer chains. Second, the molar extinction coefficients of the bis(acylphosphine oxide) photoinitiators increase gradually with increasing glycol chain length, while the absorption ranges remain nearly identical. This indicates that chain length mainly modulates absorption intensity rather than the absorption profile. Third, the fluorescence quantum yields of all these bis(acylphosphine oxide) photoinitiators are low, consistent with the behavior reported for BTPO1–3. Fourth, the migration levels of all the bis(acylphosphine oxide) photoinitiators are below the detection limit, in agreement with the undetectable migration reported in Reference [29]. Fifth, with respect to photoinitiation efficiency, under LED@405 nm irradiation the efficiency increases with increasing molecular weight, so that the higher-molecular-weight bis(acylphosphine oxide) structures exhibit higher photoinitiation efficiency. Finally, regarding monomer solubility, the viscosity of the photoinitiators increases gradually with increasing molecular weight, and all compounds remain liquids. Taken together, extending the glycol chain length from the 3–7 range of [29] to 5–9 in the present work shows that chain length can be used to tune extinction coefficient, viscosity, and photoinitiation efficiency while preserving low fluorescence and undetectable migration, thereby providing a broader structure–property map for this class of glycol-linked bis(acylphosphine oxide) photoinitiators.

3. Conclusions

This study presents four novel bifunctional macromolecular acylphosphine oxide photoinitiators with low migration properties, designed for UV-LED applications. They exhibit good photopolymerization performance, low migration, and high solubility in common monomers. BTBOLs possess a diacylphosphine oxide structure, and their maximum molar extinction coefficient is more than twice that of TPO-L. Under 356nm and 405nm LED irradiation, the DC rates of BTBOLs are higher than that of TPO-L except BTBOL-2. Meanwhile, the macromolecular photoinitiators with a bifunctional acyl-oxo structure have a molecular weight ranging from 777.31 to 953.41 g/mol, which is much higher than that of TPO-L (316.34 g/mol). The migration rate of BTBOLs was 0.00%, which was below the detection limit and much lower than that of TPO-L (0.98%). In summary, the BTBOLs appear as light yellow transparent liquids and offer a combination of low migration, good monomer solubility, and high photoinitiation efficiency. These properties make them attractive candidates for low-migration UV-LED curing applications and are expected to stimulate further development of UV-LED photopolymerization technology.

Supplementary Materials: The following supporting information can be downloaded at: https://www.mdpi.com/article/10.3390/polym18232996/s1, Figure S1: 1H NMR spectrum of BTBOL-1. Figure S2: 13C NMR spectrum of BTBOL-1. Figure S3: 31P NMR spectrum of BTBOL-1. Figure S4: 1H NMR spectrum of BTBOL-2. Figure S5: 13C NMR spectrum of BTBOL-2. Figure S6: 31P NMR spectrum of BTBOL-2. Figure S7: 1H NMR spectrum of BTBOL-3. Figure S8: 13C NMR spectrum of BTBOL-3. Figure S9: 31P NMR spectrum of BTBOL-3. Figure S10: 1H NMR spectrum of BTBOL-4. Figure S11: 13C NMR spectrum of BTBOL-3. Figure S12: 31P NMR spectrum of BTBOL-4. Figure

S13: High resolution mass spectrum of intermediate 2. Figure S14: High resolution mass spectrum of BTBOL-1. Figure S15: High resolution mass spectrum of BTBOL-2. Figure S16: High resolution mass spectrum of BTBOL-3. Figure S17: High resolution mass spectrum of BTBOL-4; Table S1: Solubility of BTBOLs in monomers. References [49,50] are cited in the Supplementary Materials.

Author Contributions: Conceptualization, Y.W. and A.G.; Methodology, Y.W.; Formal analysis, Z.Z., S.Z. and Y.L.; Investigation, Z.Z., S.Z. and Y.L.; Data curation, S.Z. and Y.L.; Writing—original draft, Y.W.; Writing—review & editing, Y.W., A.G., B.Z. and Xiang Li; Project administration, Y.W., B.Z. and X.L.; Funding acquisition, B.Z. and X.L. All authors have read and agreed to the published version of the manuscript.

Funding: This work was funded by [Zhaoqing College youth project] grant number [QN202445]; and [Zhaoqing College students innovation and entrepreneurship training program] grant number [S202510580061]. and [the Zhaoqing City Science and Technology Innovation Guidance Project] grant number [250826200811035]; [Science and Technology Innovation Guidance Projects of Zhaoqing City] grant number [241217144169263]. [Zhaoqing University Innovative Research Team Funding Program] grant number [TD202413].

Institutional Review Board Statement: Not applicable.

Data Availability Statement: The original contributions presented in this study are included in the article/Supplementary Material. Further inquiries can be directed to the corresponding authors.

Conflicts of Interest: The authors declare no conflict of interest.

References

1. Yagci, Y.; Jockusch, S.; Turro, N.J. Photoinitiated Polymerization: Advances, Challenges, and Opportunities. *Macromolecules* **2010**, *43*, 6245–6260. [CrossRef]
2. Yeow, J.; Boyer, C. Photoinitiated Polymerization-Induced Self-Assembly (Photo-PISA): New Insights and Opportunities. *Adv. Sci.* **2017**, *4*, 1700137. [CrossRef]
3. Chen, M.; Zhong, M.; Johnson, J.A. Light-Controlled Radical Polymerization: Mechanisms, Methods, and Applications. *Chem. Rev.* **2016**, *116*, 10167–10211. [CrossRef]
4. Godleman, J.; Babra, T.S.; Afsar, A.; Kyriacou, A.; Thompson, M.; Harries, J.L.; Colquhoun, H.M.; Hayes, W. Functionalised PEGs with photo-dimerisable, anthracenyl end-groups: New UV-curable materials for use in inkjet formulations. *Prog. Org. Coat.* **2021**, *151*, 106105. [CrossRef]
5. Rawat, R.S.; Chouhan, N.; Talwar, M.; Diwan, R.K.; Tyagi, A.K. UV coatings for wooden surfaces. *Prog. Org. Coat.* **2019**, *135*, 490–495. [CrossRef]
6. Sanai, Y.; Ninomiya, T.; Arimitsu, K. Improvements in the physical properties of UV-curable coating by utilizing type II photoinitiator. *Prog. Org. Coat.* **2021**, *151*, 106038. [CrossRef]
7. Bialas, S.; Michalek, L.; Marschner, D.E.; Krappitz, T.; Wegener, M.; Blinco, J.; Blasco, E.; Frisch, H.; Barner-Kowollik, C. Access to Disparate Soft Matter Materials by Curing with Two Colors of Light. *Adv. Mater.* **2019**, *31*, 1970056. [CrossRef]
8. Han, D.; Yang, C.; Fang, N.X.; Lee, H. Rapid Multi-Material 3D Printing with Projection Micro-Stereolithography Using Dynamic Fluidic Control. *Addit. Manuf.* **2019**, *27*, 606–615. [CrossRef]
9. Kolb, C.; Lindemann, N.; Wolter, H.; Zeininger, H.; Stampfl, J.; Liska, R. 3D-printing of highly translucent ORMOCER-based resin using light absorber for high dimensional accuracy. *J. Appl. Polym. Sci.* **2021**, *138*, 49691. [CrossRef]
10. Yang, G.; Zou, B.; Wang, X.; Hu, Y.; Huang, C. Study of a high solid content Mn-Zn ferrite ceramic paste system based on SLA printing and its light curing mechanism. *Ceram. Int.* **2025**, *18*, 51. [CrossRef]
11. Long, Y.; Huang, G.; Liu, S.; Xu, L.; Li, A.; Qiu, D.; Dong, Y. Hygroscopic bioactive light-cured composite promoting dentine bridge formation. *Regen. Biomater.* **2024**, *11*, rbae114. [CrossRef]
12. Lu, G.; Tang, R.; Nie, J.; Zhu, X. Photocuring 3D Printing of Hydrogels: Techniques, Materials, and Applications in Tissue Engineering and Flexible Devices. *Macromol. Rapid Commun.* **2024**, *45*, 2300661. [CrossRef]
13. Lee, J.H.; Park, S.; Lim, J.T.; Yoon, H.S.; Choi, J.W.; Ha, C.W.; Park, J. Quick-Delivery Mold Fabricated via Stereolithography to Enhance Manufacturing Efficiency. *Micromachines* **2024**, *15*, 1345. [CrossRef]
14. Yang, X.; Fang, X.; Yang, Z. Application of UV LED light-curing resin in wood field—A review. *Prog. Org. Coat.* **2026**, *217*, 110251. [CrossRef]
15. Wang, X.; Cai, X.; Hu, J.; Li, J.; Zhou, R.; Lin, S. Green synthesis of soybean oil-derived UV-curable resins for high-resolution 3D printing. *Addit. Manuf.* **2024**, *95*, 104543. [CrossRef]

16. Tosto, C.; Saitta, L.; Latteri, A.; Blanco, I. Development of recyclable bio-based epoxy/acrylate blends for liquid crystal display 3D printing. *J. Therm. Anal. Calorim.* **2025**, *150*, 6685. [CrossRef]
17. Dietlin, C.; Schweizer, S.; Xiao, P.; Zhang, J.; Morlet-Savary, F.; Graff, B.; Fouassier, J.P.; Lalevée, J. Photopolymerization upon LEDs: New photoinitiating systems and strategies. *Polym. Chem.* **2015**, *6*, 3895–3912. [CrossRef]
18. Eibel, A.; Radebner, J.; Haas, M.; Fast, D.E.; Freißmuth, H.; Stadler, E.; Faschauner, P.; Torvisco, A.; Lamparth, I.; Moszner, N.; et al. From mono- to tetraacylgermanes: Extending the scope of visible light photoinitiators. *Polym. Chem.* **2018**, *9*, 38–47. [CrossRef]
19. Hola, E.; Ortyl, J.; Jankowska, M.; Pilch, M.; Galek, M.; Morlet-Savary, F.; Graff, B.; Dietlin, C.; Lalevée, J. New bimolecular photoinitiating systems based on terphenyl derivatives as highly efficient photosensitizers for 3D printing application. *Polym. Chem.* **2020**, *11*, 922–935. [CrossRef]
20. Bednarczyk, P.; Rożniakowski, K. The Influence of the Photoinitiating System on Residual Monomer Contents and Photopolymerization Rate of a Model Pigmented UV/LED Nail Gel Formulation. *Coatings* **2025**, *15*, 1125. [CrossRef]
21. Müller, S.M.; Schlögl, S.; Wiesner, T.; Haas, M.; Griesser, T. Recent Advances in Type I Photoinitiators for Visible Light Induced Photopolymerization. *ChemPhotoChem* **2022**, *6*, e202200091. [CrossRef]
22. Navickas, M.; Skliutas, E.; Kölbel, J.; Fernández-Terán, R.J.; Malinauskas, M.; Vengris, M. Uncovering the photoexcited dynamics in bis(acyl)phosphine oxide photoinitiators. *Phys. Chem. Chem. Phys.* **2025**, *27*, 20592–20601. [CrossRef]
23. Zhao, D.; Liu, Y.; Wang, Q.; Zhang, Y.; Zhang, X.; Du, Y.; Wang, T. Acylphosphine oxide photoinitiators containing Si with sulfhydryl bridge linkages. *Prog. Org. Coat.* **2024**, *187*, 108110. [CrossRef]
24. Martín-Sómer, M.; Pablos, C.; van Grieken, R.; Marugán, J. Influence of light distribution on the performance of photocatalytic reactors: LED vs. mercury lamps. *Appl. Catal. B Environ.* **2017**, *215*, 1–7. [CrossRef]
25. Yang, T. LED replace mercury lamps for ultraviolet photofunctionalization on titanium surface. *Int. Dent. J.* **2025**, *75*, 105084. [CrossRef]
26. Liu, Y.; Wang, T.; Xie, C.; Tian, X.; Song, L.; Liu, L.; Wang, Z.; Yu, Q. Naphthyl-Based Acylphosphine Oxide Photoinitiators with High Effiency and Low Migration. *Prog. Org. Coat.* **2020**, *142*, 105603. [CrossRef]
27. Yin, J.; Zhang, Y.; Graff, B.; Dietlin, C.; Schmitt, M.; Morlet-Savary, F.; Petithory, T.; Pieuchot, L.; Zhang, J.; Peng, X.; et al. Novel Non-Cytotoxic Acylphosphinates and Acylphosphine Oxides Photoinitiators. *Angew. Chem.* **2026**, *65*, e6797341. [CrossRef]
28. Wiesner, T.; Haas, M. Do Germanium-Based Photoinitiators Have the Potential to Replace the Well-Established Acylphosphine Oxides? *Dalton Trans.* **2021**, *50*, 12392–12398. [CrossRef]
29. Wu, Y.; Dai, C.; Ke, J.; Tang, R.; Wang, J.; Huang, C.; Situ, Y.; Huang, H. Synthesis and characterization of low-migration bisacylphenylphosphine xide photoinitiators. *Prog. Org. Coat.* **2023**, *176*, 107396. [CrossRef]
30. Wu, Y.; Chi, J.; Huang, H. Bis(acylphosphine oxide) Photoinitiator and Its Preparation Method and Application: CN115448948A[P]. 2022-12-09.
31. Menti-Platten, M.; Burns, B.R.; Shiels, O.J.; Barker, P.J.; Keller, P.A.; Trevitt, A.J. Beyond Absorption: Online Photoreactor Mass Spectrometry Assessment of New Acylphosphine Oxide Photoinitiators. *Chem. Sci.* **2025**, *16*, 14625–14634. [CrossRef]
32. Peng, Z.; Shen, Q.; Chen, X. Cyclo-Bis(Acyl)phosphine Oxides as Efficient Photoinitiators for Radical Polymerization. *Eur. J. Inorg. Chem.* **2024**, *27*, e202400153. [CrossRef]
33. Thny, D.; Brack, E.; Yuts, Y.; Baruffaldi, D.; Frascella, F.; Cosola, A.; Sun, X.; Chiappone, A.; Bao, Y.; Grützmacher, H. Solvent-free 3D printing of silicone elastomers by digital light processing using an oligosiloxanyl substituted bis(acyl)phosphane oxide as photoinitiator. *Mater. Adv.* **2026**, *7*, 4128–4137. [CrossRef]
34. Xie, G.; Shuai, Z.; Huang, Y.; Yu, M.; Zeng, Z.; Yang, J. Use of floating acylphosphine oxide-based photoinitiators to reduce surface oxygen inhibition of UV-LED photopolymerization. *Prog. Org. Coat.* **2020**, *147*, 105716. [CrossRef]
35. Dietlin, C.; Trinh, T.T.; Schweizer, S.; Graff, B.; Morlet-Savary, F.; Noirot, P.-A.; Lalevée, J. New Phosphine Oxides as High Performance Near-UV Type I Photoinitiators of Radical Polymerization. *Molecules* **2020**, *25*, 1671. [CrossRef]
36. Ren, X.; Liu, W.; Yao, Q.; Wang, S.; Liu, W.; Gu, H.; Wang, D.; Fan, J.; Peng, X. A UV-LED excited photoinitiator with low toxicity and low migration for photocurable inks. *Dye. Pigment.* **2022**, *200*, 110133. [CrossRef]
37. Canellas, E.; Nerin, C.; Vera, P. Beyond direct contact: Chemical migration from external printed components of tea packaging into infusions assessed by UPLC-IM-QTOF analysis. *Food Packag. Shelf Life* **2025**, *52*, 101658. [CrossRef]
38. Qian, C.; Bai, L.; Wang, W.; Luo, Y.; Li, J.; Wang, Y. Occurrences and migration characteristics of photoinitiators in paper food packaging: Implication for human exposure. *J. Environ. Sci.* **2025**, *158*, 435–446. [CrossRef]
39. Hou, X.; Han, Y.; Li, H.; Gao, M.; Cao, Y. Migration studies of photoinitiators with different volatilities from plastic packaging to milk powder. *Anal. Chim. Acta* **2026**, *1418*, 345808. [CrossRef]
40. Ma, G.; Luo, J.; Qu, J. Synthesis and properties of acyldiphenylphosphine oxides photoinitiators carrying triphenylamine or pyrene group for free radical photopolymerization. *J. Appl. Polym. Sci.* **2023**, *140*, e54351. [CrossRef]
41. Ma, G.; Luo, J.; Qu, J. Long-wavelength absorbing photoinitiators based phenothiazine acyldiphenylphosphine oxides for free radical photopolymerization. *Prog. Org. Coat.* **2024**, *189*, 108296. [CrossRef]

42. Wu, Y.; Ke, J.; Dai, C.; Wang, J.; Huang, C.; Situ, Y.; Huang, H. Large-molecular-weight acyldiphenylphosphine oxides as low-mobility type I photoinitiator for radical polymerization. *Eur. Polym. J.* **2022**, *175*, 111380. [CrossRef]
43. Wu, Y.; Li, R.; Ke, J.; Cheng, X.; Tang, R.; Situ, Y.; Huang, H. Study on bifunctional acyldiphenylphosphine oxides photoinitiator for free radical polymerization. *Eur. Polym. J.* **2022**, *168*, 111093. [CrossRef]
44. Breloy, L.; Negrell, C.; Mora, A.S.; JenniferLi, W.S.; Brezová, V.; Caillol, S.; Versace, D.L. Vanillin derivative as performing type I photoinitiator. *Eur. Polym. J.* **2020**, *132*, 109727. [CrossRef]
45. Bassenheim, D.; Knaipp, K.; Schmallegger, M.; Gescheidt, G.; Rist, K.; Moszner, N.; Catel, Y.; Liska, R.; Knaack, P. Substituent Effects in Monoacylphosphine Oxide Photoinitiators: Efficiency and Performance. *J. Polym. Sci.* **2025**, *63*, 2167–2173. [CrossRef]
46. Yin, J.; Zhang, Y.; Graff, B.; Dietlin, C.; Schmitt, M.; Morlet-Savary, F.; Petithory, T.; Pieuchot, L.; Zhang, J.; Xu, Y.; et al. 2,4,6-Trimethylbenzoyldiphenylphosphine oxide(TPO) analog: A non-cytotoxic type-I photoinitiator for free radical photopolymerization. *Green Chem.* **2025**, *27*, 1451–1465. [CrossRef]
47. Duan, H.; Leng, K.; Xu, X.; Li, Q.; Liu, D.; Han, Y.; Gao, J.; Yu, Q.; Wang, Z. Monoacylphosphine oxides with substituents in the phosphonyl moiety as Norrish I photoinitiators: Synthesis, photoinitiation properties and mechanism. *J. Photochem. Photobiol. A Chem.* **2021**, *421*, 113517. [CrossRef]
48. Fan, J.; Hu, M.; Zhan, P.; Peng, X. Energy transfer cassettes based on organic fluorophores: Construction and applications in ratiometric sensing. *Chem. Soc. Rev.* **2013**, *42*, 29–43. [CrossRef]
49. Jockusch, S.; Koptyug, I.V.; McGarry, P.F.; Sluggett, G.W.; Turro, N.J.; Watkins, D.M. A steady-state and picosecond pump-probe investigation of the photophysics of an acyl and a bis(acyl)phosphine oxide. *J. Am. Chem. Soc.* **1997**, *119*, 11495–11501. [CrossRef]
50. Dietlin, C.; Trinh, T.T.; Schweizer, S.; Graff, B.; Morlet- Savary, F.; Noirot, P.A.; Lalevée, J. Rational design of acyldiphenylphosphine oxides as photoinitiators of radical polymerization. *Macromolecules* **2019**, *52*, 7886–7893. [CrossRef]

Disclaimer/Publisher's Note: The statements, opinions and data contained in all publications are solely those of the individual author(s) and contributor(s) and not of MDPI and/or the editor(s). MDPI and/or the editor(s) disclaim responsibility for any injury to people or property resulting from any ideas, methods, instructions or products referred to in the content.